

Nanoscale

Accepted Manuscript



This is an *Accepted Manuscript*, which has been through the Royal Society of Chemistry peer review process and has been accepted for publication.

Accepted Manuscripts are published online shortly after acceptance, before technical editing, formatting and proof reading. Using this free service, authors can make their results available to the community, in citable form, before we publish the edited article. We will replace this *Accepted Manuscript* with the edited and formatted *Advance Article* as soon as it is available.

You can find more information about *Accepted Manuscripts* in the [Information for Authors](#).

Please note that technical editing may introduce minor changes to the text and/or graphics, which may alter content. The journal's standard [Terms & Conditions](#) and the [Ethical guidelines](#) still apply. In no event shall the Royal Society of Chemistry be held responsible for any errors or omissions in this *Accepted Manuscript* or any consequences arising from the use of any information it contains.

**A new phase transformation path from nanodiamond to
new-diamond via an intermediate carbon onion**

J. Xiao [†], J. L. Li [†], P. Liu & G. W. Yang ^{*}

*State Key Laboratory of Optoelectronic Materials and Technologies, Institute of
Optoelectronic and Functional Composite Materials, Nanotechnology Research
Center, School of Physics & Engineering, Sun Yat-sen University, Guangzhou 510275,
Guangdong, P. R. China*

[†] These authors contributed equally to this work.

^{*} Corresponding author: stsygw@mail.sysu.edu.cn

Abstract

The investigation of carbon allotropes such as graphite, diamond, fullerenes, nanotubes and carbon onion and mechanisms that underlie their mutual phase transformation is a long-standing problem of great fundamental importance. New diamond (n-diamond) is a novel metastable phase of carbon with a face-centered cubic structure, being called “new diamond” because many reflections in its electron diffraction pattern are similar to those of diamond. However, producing n-diamond from raw carbon materials has been so far challenging due to n-diamond’s higher formation energy than that of diamond. Here, we, for the first time, demonstrate a new phase transformation path from nanodiamond to n-diamond via an intermediate carbon onion in the unique process of laser ablation in water, and establish that water plays a crucial role in the formation of n-diamond. When laser irradiates colloidal suspensions of nanodiamonds at ambient pressure and room temperature, nanodiamonds are firstly transformed into carbon onions serving as an intermediate phase, and sequentially carbon onions are transformed into n-diamonds driven by the laser-induced high-temperature and high-pressure from the carbon onion as a nanoscaled temperature and pressure cell upon the process of laser irradiation in liquid. This phase transformation not only gains a new insight into the physical mechanism involved, but also offers one suitable opportunity for breaking controllable pathways between n-diamond and carbon allotropes such as diamond and carbon onion.

1. Introduction

The phase transformation between diamond and other carbon allotropes, for example, graphite, fullerenes, nanotubes and carbon onion, has been of intense interest from the viewpoints of science and technology for a century, and breaking controllable pathways between diamond and these carbon allotropes is a subject that has fascinated scientists and engineers for several decades¹⁻¹⁰. Among the multifarious carbon allotropes, a novel metastable phase of carbon with the face-centered cubic (fcc) structure has been produced by some techniques under extreme conditions¹¹⁻¹³. This unique form of carbon is called new diamond (n-diamond) because many reflections in its electron diffraction pattern are similar to those of diamond¹¹. In recent years, this metastable phase of carbon has attracted considerable interest because researchers have demonstrated that n-diamond actually presents a new kind of metastable phases of carbon with the fcc structure and is expected to have great potential applications in areas of mechanical engineering, microelectronics and optoelectronics¹¹⁻¹⁵. Therefore, there is a growing interest in breaking controllable pathways between n-diamond and other carbon allotropes including graphite and diamond. However, producing n-diamond from raw carbon materials has been so far challenging due to n-diamond's higher formation energy than that of diamond¹⁶.

Here, we, for the first time, demonstrate a new phase transformation pathway from nanodiamond to n-diamond via an intermediate carbon onion driven by the process of laser ablation in water, and we establish that water plays a crucial role in the formation of n-diamond. These results reveal a series of phase transformations

between n-diamond and other carbon allotropes such as diamond and carbon onion, and having a clear and general insight into the basic physics involved in these conversions. Meanwhile, this phase transformation path from diamond to n-diamond opens up avenues for producing n-diamond from raw carbon materials.

2. Experimental

In our study, raw detonation nanodiamonds (Aldrich, $\geq 97\%$ trace metals basis, nanopowder) synthesized from the detonation of the mixture of trinitrotoluene and hexogen⁹ and deionized water are used without further purification. The experiments are carried out in the system of laser ablation in liquid^{17,18}. In this case, about 3 mg raw detonation nanodiamonds are dropped into 10 mL bottle filled with deionized water to form the suspension. Then, a second harmonic produced by a Q-switched Nd:YAG laser device with a wavelength of 532 nm, pulse width of 10 ns, repeating frequency of 10 Hz, and laser pulse power of 200 mJ is focused into the middle of the bottle with 1 mm beam size. During the laser irradiation, the solution is kept stirring with a magnetic stirrer. After the ablation, one drop of different periods of the solution is pipetted onto a carbon support film on a copper grid for transmission electron microscopy (TEM) observation. TEM and High resolution transmission electron microscopy (HRTEM) images are recorded using an FEI Tecnai G2 F30 transmission electron microscope equipped with a field-emission gun. The electron energy loss spectroscopy (EELS) studies are recorded by using an imaging filter (Gatan GIF) in the TEM imaging mode. The energy resolution of the system is 1 eV (FWHM of

zero-loss peak) and the maximum dispersion is 0.05 eV per channel.

All the theoretical calculations are performed using the DMOL package. Spin unrestricted calculations in the generalized gradient approximation (GGA) with the Perdew–Burke–Ernzerhof (PBE) exchange-correlation function are used. The atomic orbital basis set is of double-numerical quality with inclusion of polarization functions (DNP). The configurations are fully relaxed without any symmetric constraints until the maximal forces are less than 0.002 hartree / Å. The Kohn–Sham equations are solved self-consistently with a convergence of 10^{-5} Ha on the total energy. The potential energy profile of the face-centered cubic carbon is scanned by different lattice constants. The completely same theoretical-level calculations are performed for diamond.

The EELS of the face-centered cubic carbon is calculated using the Castep package. The calculations adopted the GGA with the PBE exchange-correlation function. The Kohn–Sham equations are solved self-consistently with a convergence of 10^{-5} Ha (1Ha=27.2116eV) on the total energy. The kinetic energy cut-off is 350 eV. A core hole calculation is performed, in a $3 \times 3 \times 3$ supersell to ensure one single cell only containing one full core hole. The Pseudopotential constructed for an atom missing a core electron is on the fly (OTFG) and in the representation of reciprocal space. To insure this issue, we carry out the same theoretical-level calculation for the EELS of diamond.

3. Results and Discussion

Figure 1a shows the typical morphology of aggregated raw nanodiamonds with the size of about 5 nm. Four strong diffraction rings (Figure 1b) represent the (111), (220), (311), (400) planes of diamond. HRTEM image of raw nanodiamonds are consisting of the crystalline diamond cores and the amorphous outer shells as shown in Figure 1c. Scanning transmission electron microscopy (STEM) (Figure 1(d-e)) and TEM image (Figure 1 (g-h)) demonstrate that the as-synthesized products are turn out to be the nanoparticles with diameters of 30-40 nm and these nanoparticles are in the shape of nanospheres connected with each other. In spite of the closeness of the crystal lattice parameter of the phase to that of diamond, its selected area electron diffraction (SAED) pattern significantly differs from that of diamond as shown in Figure 1f. Four strong diffraction rings denote the (111), (200), (220) and (311) planes of n-diamonds. Note that, the (200) ring of n-diamond is forbidden for diamond¹⁹. Based on the HRTEM image of n-diamonds (Figure 1i), we can see that these n-diamonds are found to be embedded into the disorder carbons. This phenomenon is concerned with the stability of sp^3 bonding, which is detailed discussed below. The ratio between amorphous carbon and n-diamond is roughly estimated to be 7:3. Besides, some nanodiamonds are consumed in other ways, such as vaporization and transforming to organic groups when subjected to the laser ablation. Therefore, combining these influencing factors, the percent conversion between raw diamond and n-diamond is approximately 10%. Furthermore, the HRTEM analysis of the individual n-diamond (Figure 1j-k) shows that the two interplanar spacings of 0.313 and 0.272 nm, respectively, correspond to the crystallographic planes of the (111) and

(200) of the fcc structure quite well. In addition, an angle of $\Phi=125^\circ$ between the two interplanar spacings further confirms that the as-synthesized samples possess a fcc structure with the lattice parameter of 0.545 nm. Accordingly, TEM data demonstrate a phase transformation from diamond to n-diamond. Note that the n-diamond synthesized by this method is different from the common n-diamond reported by other literatures¹¹⁻¹⁵. The difference between these three diamonds structures have been listed in Table 1. Additionally, we compare estimate the stability among them by introducing first-principles calculation, and these results show that the n-diamond in our case is higher 0.65 and 1.05 Ha (1Ha=27.2116eV) than that of common n-diamond and diamond, respectively, on the total formation energy, which means that the n-diamond with larger lattice parameter ($a=0.545$ nm) in our case is a metastable state compared to other two diamonds ($a=0.356$ nm) (the detailed calculation in theoretical section below).

In order to detailed elucidate the phase transformation process above, we carefully check the products at different irradiation of laser stage and find out the intermediate products during from diamond to n-diamond transiting. The irradiation time of nine bottles of Figure 2e is 0, 5, 10, 15, 20, 45, 60, 70 and 90 min, respectively. The sample of the final products is from 9th bottle in Figure 2e. HRTEM images of the intermediate products in Figure 2 exhibit that various morphologies of carbon onions (the sample from 5th bottle in Figure 2e) are found including quasi-spherical particles, polyhedron particles with closed concentric graphite shells, and elongated particles with linked external graphite-like layers. Clearly, the spacing of the lattice fringes is

about 0.34 nm, corresponding to that of the (002) plane of graphite. These results thus show that raw nanodiamonds are firstly transformed into carbon onions serving as an intermediate phase, and sequentially carbon onions are transformed into n-diamonds in the process of laser irradiation in liquid. During the laser irradiating, we can clearly see a series of significant color changes of the colloid from opaque grayish white to dark black and finally to a transparent colorless as shown Figure 2e. Note that, the intermediate phase are black both in water and alcohol environment¹⁷, which indicate that carbon onions definitely regard as the transient phases from raw nanodiamonds to the final products no matter what kind of liquid.

Figure 3a shows the EELS spectra of nanodiamond, carbon onion and n-diamond, respectively. The curve i in Figure 3a gives a characteristic diamond peak > 290 eV, due to the transition from the 1s core level to the σ^* band ($1s \rightarrow \sigma^*$ transition)²⁰, apart from the presence of a weak peak at 284.8 eV ($1s \rightarrow \pi^*$ transition). These results indicate the presence of some sp^2 -bonded carbon atoms, which is verified by TEM observation in Figure 1c. Despite the ordered network of carbon onions observed in HRTEM images (Figure 2(a-d)), this EELS analysis characterized by the carbon K edge (the curve ii in Figure 3) resembles that obtained from amorphous carbon²¹. The broadened peak at 284.8 eV, corresponding to the transition from the 1s core level to the π^* band ($1s \rightarrow \pi^*$ transition), and no obvious peak appear above 290 eV, suggesting that sp^3 bonds transform to sp^2 ones. This phenomenon corresponds well to that of Tomita's research²². In the spectrum of n-diamonds (the curve iii in Figure 3), we can see a shoulder at about 284.8 eV. The disorder carbons as shown in Figure 1i are

considered to be responsible for the shoulder. However, the fine structure above the $1s \rightarrow \sigma^*$ transition observed for n-diamonds is significantly different from that of common nanodiamonds in the relative intensity and peak location. The three characteristic $1s \rightarrow \sigma^*$ transitions of 291.9, 297.7, and 305.3 eV have shifted to 291.7, 302.8, and 314.2 eV. In order to validate the accuracy of experimental observations, we perform the DFT calculations to simulate the EELS spectra (the detailed process in theoretical section below). Firstly, we calculate the EELS spectrum of well-known diamond as shown in Figure 3b. Clearly, the theoretical results are consistent with the experimental measurement. Therefore, this simulation method is recognized to be convincing and reliable. Then, the EELS spectrum of n-diamond is calculated based on the same method as shown in Figure 3c. The shape and relative intensity of three peaks are basically the same as that of the experimental profile. Although the theoretical values of peak locations are in disparity with the experimental values due to the calculation issues, it would not influence the precision in judging the shape and relative intensity of peaks, which have been validated by testing the EELS spectrum of diamond (Figure 3b). Therefore, combining experimental and theoretical data, we convince that the products are n-diamonds with a face-centre cubic structure.

To further convince the phase transformation processes, we utilize the UV Raman (325nm) to analyse samples collected at different stages, as shown in Figure 4. Raw detonation nanodiamonds (bottom) show a peak at 1325 cm^{-1} , which belong to typical signal of diamond⁹ and the G band peaks around 1600 cm^{-1} . After 20min ablation, the diamond peak upshifts to about 1410 cm^{-1} , which is attributed to the

disorder sp^2 -bonded carbon phase (D band)²³. Besides, due to the effect of the shell curvature of carbon onions, the G band downshifts to 1585 cm^{-1} (middle)²⁴. Finally, the D band moves down to 1363 cm^{-1} (top). Although the amorphous carbon around n-diamond has some influence in the final Raman signal of n-diamond, the downshift of D band is still considered to be ascribed to the appearance of increase of sp^3 bonding when generating n-diamonds¹⁷.

Based on above the detailed characterizations, the as-synthesized products are convinced to be the n-diamond by laser ablating raw detonation nanodiamonds in deionized water. However, according to our previous research¹⁷, when the liquid is absolute alcohol, the final products are traditional nanodiamonds with good monodisperse. Therefore, it is obviously that the liquid is a key factor to determinate the final carbon structures. Gogotsi *et al.* have claimed that the surface of sp^3 clusters must be either stabilized through termination with functional groups or reconstructed into sp^2 carbon⁹. In order to judge the surface termination of the products synthesized with different liquids, Fourier transform infrared spectroscopy (FTIR) of the products is introduced as shown in Figure 5. The functional groups contained in diamonds synthesized in alcohol are C=O, COOR, C-O-C, OH and C-H groups, which is much more than n-diamond having OH and little C-H and C-O groups synthesized in water. Back to Gogotsi's claim, in order to retain the stability of surface sp^3 cluster, the diamonds synthesized in the alcohol environment keep stable by means of various kinds groups adsorbed on their surface. Especially for carboxyl and carbonyl groups (not found in the water environment), they seem to easily adhere to surface of carbon

backbone^{25,26}. Due to lack of functionalities in the relatively moderate water environment, the bare (non-functionalized) or less-functionalized surfaces of the diamonds exhibit structures similar to bulk diamond. The surface of octahedral, cuboctahedral and spherical clusters show a transition from sp^3 carbon to sp^2 carbon²⁷, which corresponds with our EELS analysis and TEM observation. Thus, these results prove the existence of the disorder carbons around n-diamond, which plays an important role in the stability of n-diamonds by influencing surface reconstruction via taking shape of sp^2 carbon.

In addition, another aspect is worthy to point out, that is, the as-synthesized n-diamond has higher formation energy than that of diamond. We have successfully synthesized the cubic structure carbon by laser ablation amorphous carbon films in water such as C_8 nanocubes and body-centered cubic carbon nanocrystals^{28,29}. Recently, C_8 carbon and common n-diamonds are generated by an ArF excimer laser in the deionized water³⁰. These studies all confirm that the water environment play an important role in forming metastable carbon structures. Although the effect of water is unclear so far, hydroxyl derived from water may be attributed to prompt diamond up to a metastable with higher level. Considering FTIR results, we find out that the hydroxyl adsorbed on n-diamond is more than in the alcohol environment, which corresponds with our deductions.

Well known, carbon onion is the stable form of carbon at ambient temperatures and pressures, and both of diamond and n-diamond are metastable³¹. Thus, diamonds can be converted to carbon onions by a simply thermal annealing³². However,

according to our calculations, the formation energy of n-diamond is even higher than that of diamond, which means that n-diamond is metastable compared with diamond. Therefore, the thermodynamic driving force (high-temperature and high-pressure) is needed to push carbon onion to convert to n-diamond.

During the laser irradiating the starting nanodiamonds with thin amorphous carbon shells, laser can induce a high-temperature in the amorphous carbon shell by amorphous carbon absorbing laser energy³³. Therefore, we firstly establish a heating modal of nanoparticles upon the laser irradiating in liquid on the basis that amorphous carbon and carbon onion can absorb light and be heated³³. The energy absorbed by a nanoparticle from the laser pulse is spent in the heating process, which is described as following the equation¹⁷

$$J\sigma_{abs}^{\lambda} = m \int_{T_0}^T C_p(T) dT \quad (1)$$

where m is the particle mass, d is the diameter of particle, ρ is the density, J is laser fluence, T_0 is fixed to 300 K, σ_{abs}^{λ} is the particle absorption cross section which strongly depends on the laser wavelength, and $C_p(T)$ is the heat capacity. From the equation (1), it is clear that the amorphous carbon shell will be heated by supplied sufficient power by laser. This situation applies equally to carbon onion. Detailed theoretical modeling of laser-induced high-temperature in amorphous carbon and carbon onion can refer to Supplementary Information S1 and Figures S1-S4.

Similarly, laser can induce a high-temperature in these carbon onions by carbon onion absorbing laser energy on the basis of the proposed theoretical model. However, this laser-induced high-temperature will compress the interlayer distance of

carbon onion. Finally, the interlayer distance reducing will result in a high-pressure inside carbon onion¹⁷. Therefore, carbon onion can be regarded as a nanoscaled temperature and pressure cell upon the process of laser irradiation in liquid. A theoretical model has been developed to pursue the origin of high-pressure inside carbon onion in our case.

Considering a carbon onion consisting of a cage with radius R , the pressures (p) acting on carbon cages are^{17,34}

$$p = \frac{\rho_{\infty}^2}{4\pi R^2} \int_{S^{(0)}} \left(\int_{S^{(0)}} F dS^{(0)} \right) dS^{(0)} \quad (2)$$

where ρ_{∞} is the atom density of plane graphene, $S^{(0)}$ denote the areas carbon cages in the undeformed state which is used as a reference configuration, F are the vdW forces acting on each of the atoms (positive for the attraction). Detailed theoretical modeling of laser-induced a high-pressure environment inside the carbon onion can refer to Supplementary Information S2 and Figures S5-S7.

According to the recent review regarding transformation of carbon nanoparticles, the nucleation of diamond cores in carbon onions is observed when the onions are exposed to sustained electron irradiation above 400 °C and the pressure in the centre of the onion estimates yield pressures clearly above 10 GPa³⁵. From Figures S4 and S7, a high-temperature and high pressure induced by the laser will lead to more than 2000 °C and 20 GPa inside carbon onion. Therefore, considering a high-temperature and high-pressure environment inside carbon onion driven by the laser irradiation in liquid coupled with unique water environment discussed above, it is very reasonable to realize the carbon nanoparticles with higher formation energy than diamond, such

as n-diamond in our case.

In order to verify the possibility that whether the onions can transform to n-diamonds, we synthesize the pure carbon onions by annealing of the nanodiamonds at 1500 °C in a high vacuum chamber ($\sim 10^{-3}$ Pa) for 30min, which is similar to previous works by other authors^{21,32}. After heating treatment, the brown powder becomes dark black (Figure 6a). We take about 3mg samples into the bottle filled with deionized water and carry out the similar laser irradiation in liquid. A series of significant color changes of the colloid from dark black to a transparent colorless colloid during the laser irradiating (Figure 6b). This phenomenon of color change is identical to the latter part of Figure 2e. Sequentially, the products after annealing and final products are taken for TEM characterization. The black products are turn out to be carbon onions (Figure 6c), which in good agreement with the previous results^{21,32}. Besides, n-diamonds can still be found in final bottle, which is confirmed by HRTEM image and SAED pattern (Figure 6d). This verification test demonstrates that the onions can transform directly to n-diamond. In other word, this phase transformation mechanism from nanodiamonds to onion to n-diamond is confirmed to be evidencing and convincing.

Based on the experimental observation and the corresponding thermodynamic analysis above, the phase transformation path from diamond to n-diamond via an intermediate carbon onion in the process of laser irradiation in liquid is ascribed as shown in Figure 7. In the nanodiamond to carbon onion phase transformation upon the laser irradiation in liquid, the laser can induce a high-temperature in the

amorphous carbon shell by amorphous carbon absorbing laser energy during the laser irradiating the starting nanodiamonds with thin amorphous carbon shells. Then, the laser-induced high-temperature drives the nanodiamond core to transform into the carbon onion. Sequentially, the laser irradiates the carbon onion and then drives it into a state of high-temperature by carbon onion absorbing laser energy. Further, this high-temperature can induce a high-pressure inside the carbon onion by compressing the interlayer distance of carbon onion. Therefore, carbon onion can be served as a nanoscaled temperature and pressure cell for generation of high-temperature and high-pressure inside carbon onion upon the laser irradiation confined by liquid. Finally, the laser-induced high-temperature and high-pressure can drive the carbon onion to convert to the n-nanodiamond.

4. Conclusion

In summary, we have demonstrated a new phase transformation from nanodiamond to n-diamond via an intermediate carbon onion driven by the process of laser irradiation in water, and established the thermodynamic model to elucidate the physical mechanism involved in the experimental observations. We also demonstrate that water plays a crucial role in the formation of n-diamond. These results showed that the laser-induced high-temperature in the amorphous carbon shell of the starting nanodiamonds firstly result in the phase transformation from the nanodiamond core to the carbon onion, and then the carbon onion is converted to the n-diamond driven by the laser-induced high-temperature and high-pressure from carbon onion as a

nanoscaled temperature and pressure cell upon the process of laser irradiation in liquid. Therefore, these findings offer one suitable approach for breaking controllable pathways between n-diamond and other carbon allotropes, and open up avenues for producing n-diamonds from raw carbon materials.

Acknowledgements. The National Basic Research Program of China (2014CB931700) and the State Key Laboratory of Optoelectronic Materials and Technologies of Sun Yat-sen University supported this work.

References

1. N. R. Greiner, D. S. Phillips, J. D. Johnson, and F. Volk, *Nature*, 1988, **333**, 440–442.
2. P. Badziag, W. S. Verwoerd, W. P. Ellis, and N. R. Greiner, *Nature*, 1990, **343**, 244–245.
3. F. Banhart and P. M. Ajayan, *Nature*, 1996, **382**, 433–435.
4. A. De Vita, G. Galli, A. Canning, and R. Car, *Nature*, 1996, **379**, 523–526.
5. J.-Y. Raty and G. Galli, *Nature Mater.*, 2003, **2**, 792–795.
6. C. X. Wang, Y. H. Yang, N. S. Xu, and G. W. Yang, *J. Am. Chem. Soc.*, 2004, **126**, 11303–11306.
7. C. Wang, J. Chen, G. Yang, and N. Xu, *Angew. Chem. Int. Ed.*, 2005, **117**, 7580–7584.
8. C. X. Wang and G. W. Yang, *Mater. Sci. & Eng. R*, 2005, **49**, 157–202.
9. V. N. Mochalin, O. Shenderova, D. Ho, and Y. Gogotsi, *Nature Nanotech.*, 2012, **7**, 11–23.
10. I. I. Vlasov, A. A. Shiryaev, T. Rendler, S. Steinert, S.-Y. Lee, D. Antonov, M. Voros, F. Jelezko, A. V Fisenko, L. F. Semjonova, J. Biskupek, U. Kaiser, O. I. Lebedev, I. Sildos, P. R. Hemmer, V. I. Konov, A. Gali, and J. Wrachtrup, *Nature Nanotech.*, 2014, **9**, 54–58.
11. H. Hirai and K.-I. Kondo, *Science*, 1991, **253**, 772–774.
12. S. M. Jarkov, Y. N. Titarenko, and G. N. Churilov, *Carbon*, 1998, **36**, 595–597.
13. I. Konyashin, A. Zern, J. Mayer, F. Aldinger, V. Babaev, V. Khvostov, and M. Guseva, *Diamond Relat. Mater.*, 2001, **10**, 99–102.
14. G. Murrieta, A. Tapia, and R. de Coss, *Carbon*, 2004, **42**, 771–774.
15. M. L. Terranova, D. Manno, M. Rossi, A. Serra, E. Filippo, S. Orlanducci, and E. Tamburri, *Cryst. Growth Des.*, 2009, **9**, 1245–1249.
16. G. Baldissin and D. J. Bull, *Diamond Relat. Mater.*, 2013, **34**, 60–64.

17. J. Xiao, G. Ouyang, P. Liu, C. X. Wang, and G. W. Yang, *Nano Lett.*, 2014, **14**, 3645–3652.
18. G. W. Yang, *Prog. Mater. Sci.*, 2007, **52**, 648–698.
19. M. Fatow, I. Konyashin, V. Babaev, M. Guseva, V. Khvostov, and N. Savtchenko, *Vacuum*, 2002, **68**, 75–78.
20. Y. Gogotsi, S. Welz, D. A. Ersoy, and M. J. McNallan, *Nature*, 2001, **411**, 283–287.
21. O. O. Mykhaylyk, Y. M. Solonin, D. N. Batchelder, and R. Brydson, *J. Appl. Phys.*, 2005, **97**, 074302.
22. S. Tomita, M. Fujii, S. Hayashi, and K. Yamamoto, *Chem. Phys. Lett.*, 1999, **305**, 225–229.
23. J. Cebik, J. K. McDonough, F. Peerally, R. Medrano, I. Neitzel, Y. Gogotsi, and S. Osswald, *Nanotechnology*, 2013, **24**, 205703.
24. E. D. Obraztsova, M. Fujii, S. Hayashi, V. L. Kuznetsov, Y. V. Butenko, and A. L. Chuvilin, *Carbon*, 1998, **36**, 821–826.
25. X. Li, S. Zhang, S. A. Kulinich, Y. Liu, and H. Zeng, *Sci. Rep.*, 2014, **4**, 4976.
26. L. Wang, S.-J. Zhu, H.-Y. Wang, S.-N. Qu, Y.-L. Zhang, J.-H. Zhang, Q.-D. Chen, H.-L. Xu, W. Han, B. Yang, and H.-B. Sun, *ACS Nano*, 2014, **8**, 2541–2547.
27. A. S. Barnard, S. P. Russo, and I. K. Snook, *Diamond Relat. Mater.*, 2003, **12**, 1867–1872.
28. P. Liu, H. Cui, and G. W. Yang, *Cryst. Growth Des.*, 2008, **8**, 581–586.
29. P. Liu, Y. L. Cao, C. X. Wang, X. Y. Chen, and G. W. Yang, *Nano Lett.*, 2008, **8**, 2570–2575.
30. S. Z. Mortazavi, P. Parvin, A. Reyhani, S. Mirershadi, and R. Sadighi-Bonabi, *J. Phys. D: Appl. Phys.*, 2013, **46**, 165303.
31. R. S. Lewis, T. Ming, J. F. Wacker, E. Anders, and E. Steel, *Nature*, 1987, **326**, 160–162.
32. V. L. Kuznetsov, A. L. Chuvilin, Y. V. Butenko, I. Y. Mal'kov, and V. M. Titov, *Chem. Phys. Lett.*, 1994, **222**, 343–348.

33. K.-Y. Niu, H.-M. Zheng, Z.-Q. Li, J. Yang, J. Sun, and X.-W. Du, *Angew. Chem. Int. Ed.*, 2011, **50**, 4099–4102.
34. M. Todt, F. G. Rammerstorfer, F. D. Fischer, P. H. Mayrhofer, D. Holec, and M. A. Hartmann, *Carbon*, 2011, **49**, 1620–1627.
35. F. Banhart, *Phil. Trans. R. Soc. Lond.*, 2004, **362**, 2205–2222.

Table 1. Indexing results of SAED patterns of various diamond nanostructures

(a) diamond		a=3.56 Å	
(hkl)	$D_{\text{exp.}}$ (Å)	$D_{\text{theor.}}$ (Å)	
111	2.06	2.05	
220	1.27	1.26	
311	1.09	1.07	
400	0.90	0.89	

(b) common n-diamond [30]		a=3.56 Å	
(hkl)	$D_{\text{exp.}}$ (Å)	$D_{\text{theor.}}$ (Å)	
111	2.09	2.06	
200	1.79	1.78	
220	1.27	1.26	
311	1.10	1.07	

(c) n-diamond in our case		a=5.45 Å	
(hkl)	$D_{\text{exp.}}$ (Å)	$D_{\text{theor.}}$ (Å)	
111	3.13	3.15	
200	2.72	2.73	
220	1.92	1.93	
311	1.64	1.64	

$D_{\text{exp.}}$ refers to the experimental values. $D_{\text{theor.}}$ refers to the theoretical values. a refers to the lattice parameter.

Figure Captions

Figure 1. Microscopy characterization of nanodiamonds and n-nanodiamonds. (a) Typical morphology of aggregated raw nanodiamonds with the size of about 5 nm. (b) Four strong diffraction rings representing the (111), (220), (311), (400) planes of diamond. (c) HRTEM image of raw nanodiamonds covered by the amorphous carbon shell. (d-e) Low and high magnification STEM images of n-nanodiamonds. (f) SAED pattern of n-nanodiamonds. Four strong diffraction rings denoting the (111), (200), (220), (311) planes of n-nanodiamonds. Note that, the (200) ring is forbidden for diamond. (g-h) Low and high resolution TEM images of n-nanodiamonds. (i) HRTEM image of n-nanodiamonds. These n-nanodiamonds are found to be embedded in the disorder carbons. (j-k) HRTEM image of the individual n-nanodiamond. Detailed analysis showing the marked lattice spacing is measured to be 0.313 and 0.272 nm, respectively, which coincides with the d value of the (111) and (200) lattice planes of diamond with the face-centre cubic structure. And the interfacial angle of $\sim 125^\circ$ also confirms this structure.

Figure 2. Carbon onion serving as the intermediate phase. (a-d) The spherical carbon onions aggregated, which contain quasi-spherical particles with closed concentric graphite shell, elongated particles with linked external graphite-like layers and closed quasi-spherical internal shells. The interplanar spacing of 0.34 nm corresponds to that of the (002) plane of graphite. (e) Color change with the increase of laser irradiation

time. Clearly, the color of the solution changes from opaque greyish white to dark black and finally to transparent colorless solution.

Figure 3. EELS analysis. (a) Experimental comparison of nanodiamond, carbon onion and n-nanodiamond. All these spectra show the same peak of about 284.8 eV, meaning that these samples are involved in $1s \rightarrow \pi^*$ transition. However, they are significantly different in $1s \rightarrow \sigma^*$ transition. (b-c) The theoretical modeling of diamond and n-diamond, respectively, the inset showing the corresponding crystal structure.

Figure 4. Raman spectra analysis of the phase transformation from the raw nanodiamonds to the n-diamond. Raw detonation nanodiamonds (bottom), a peak at 1325 cm^{-1} belongs to typical signal of diamond and the G band peaks around 1600 cm^{-1} . After the appearance of carbon onion (middle), the diamond peak shifts to 1410 cm^{-1} , the G band also make a downshift to 1585 cm^{-1} . The peak at $\sim 1410 \text{ cm}^{-1}$ downshifting to 1363 cm^{-1} is associated with generating n-diamond (top), probably ascribed to the generation of increase of sp^3 bonding.

Figure 5. FTIR spectrum of products synthesized in alcohol and water, respectively, showing the samples synthesized in alcohol environment having much more functional groups than water.

Figure 6. Direct transformation from carbon onions to n-diamonds. (a) Annealing of

the brown nanodiamonds (left) at 1500°C in a high vacuum chamber, the color of products become dark black (right). (b) A series of significant color changes of the colloid from dark black to a transparent colorless during the laser irradiating. (c) The HRTEM image of products after heating treatment, which is turn out to be carbon onions. (d) The SAED pattern and HRTEM image of final products, matching with the structure of n-diamond.

Figure 7. Schematic illustration of the physical mechanism of the phase transformation from nanodiamond to n-nanodiamond. ΔG means the energy difference between two phases and ΔE means the activation energy which is essential for the phase transition from one to another one.

Figure 1

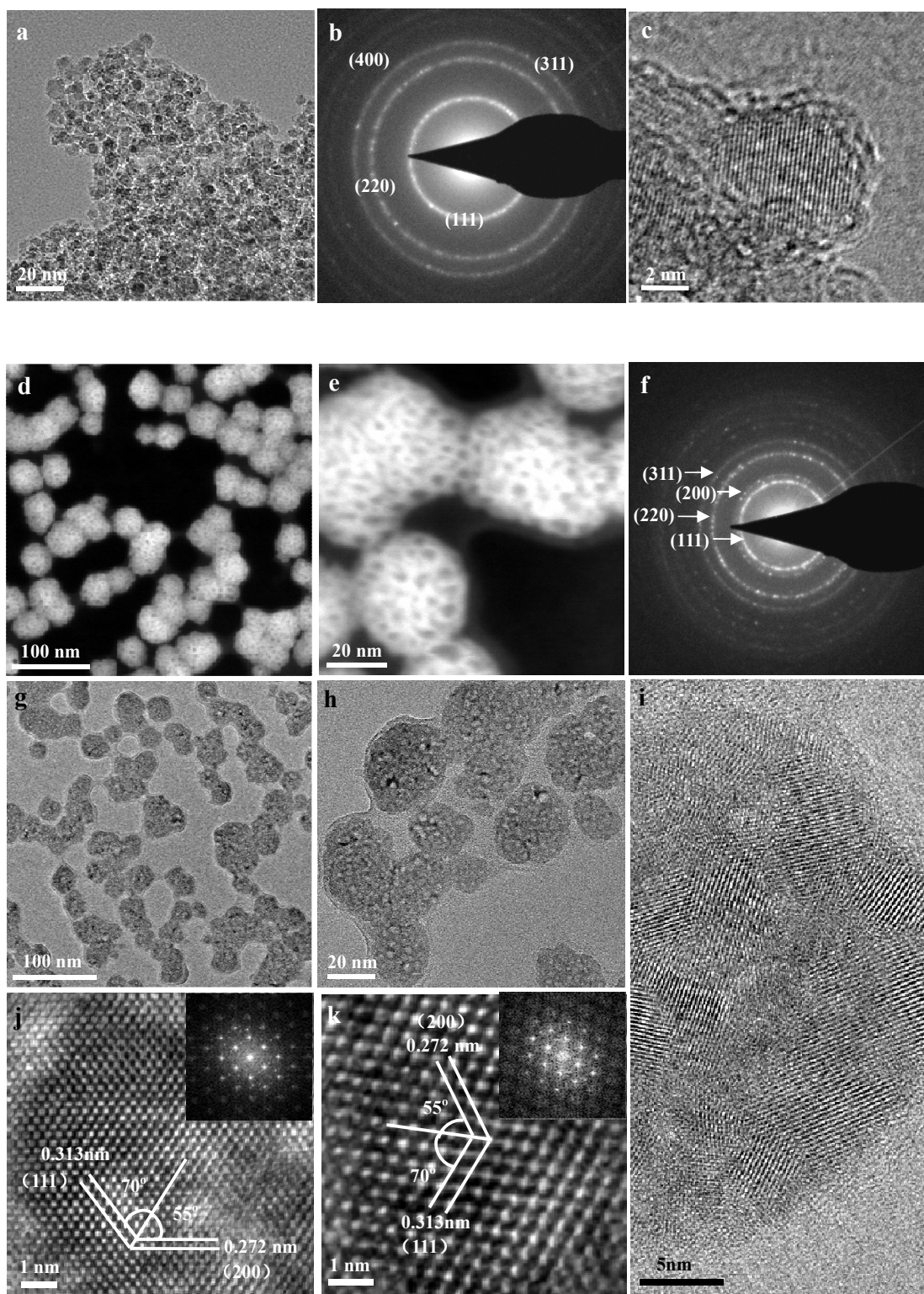


Figure 2

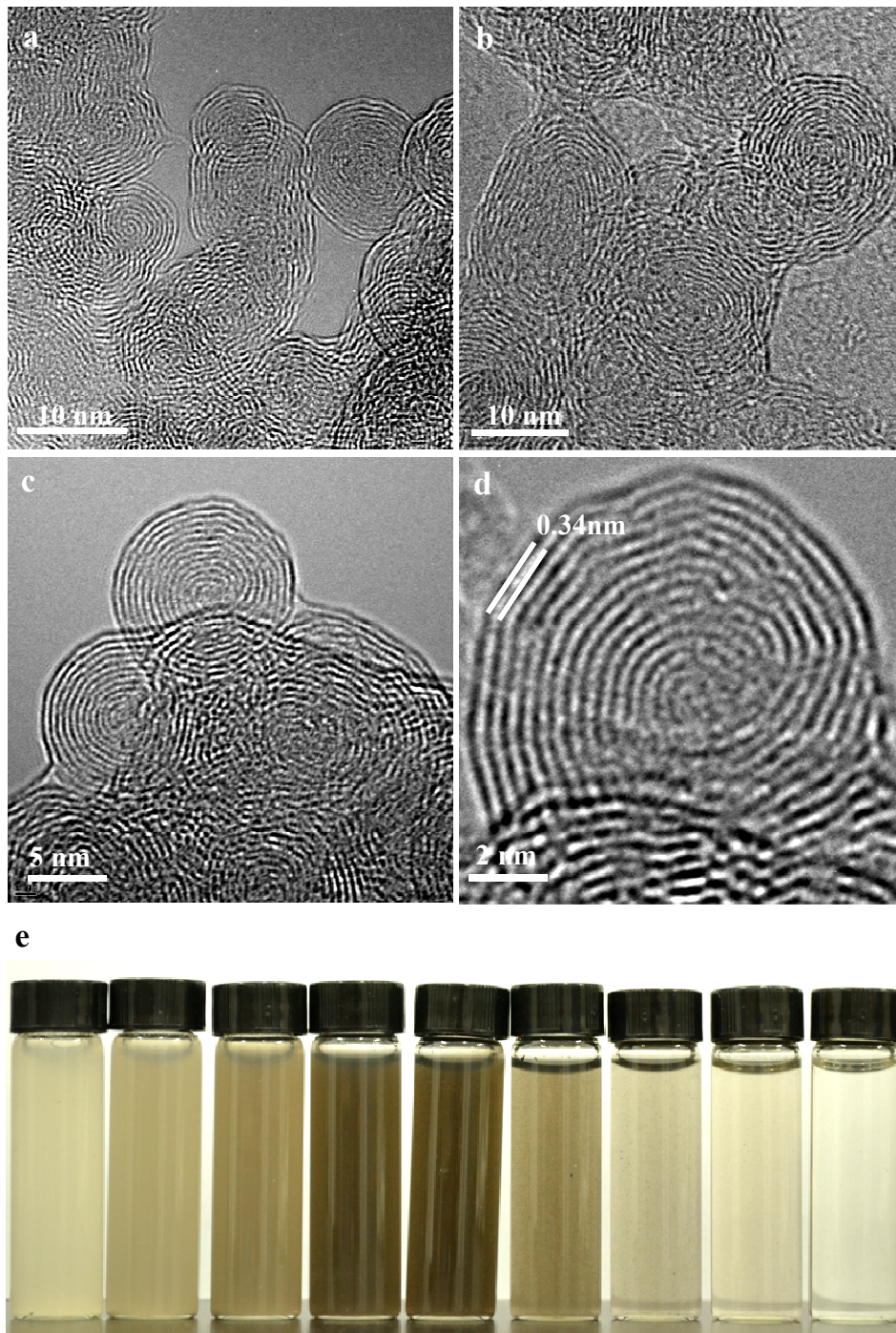


Figure 3

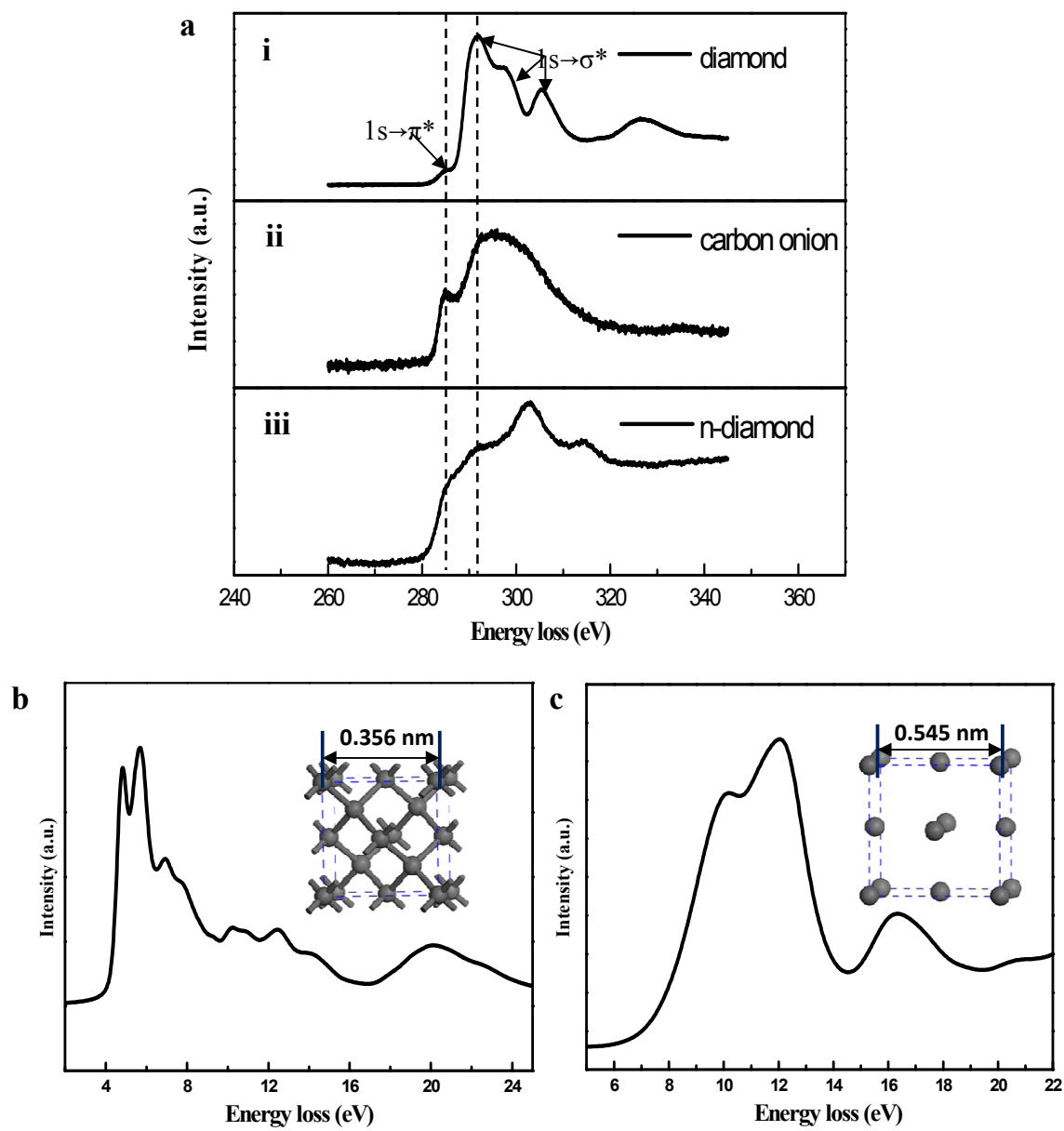


Figure 4

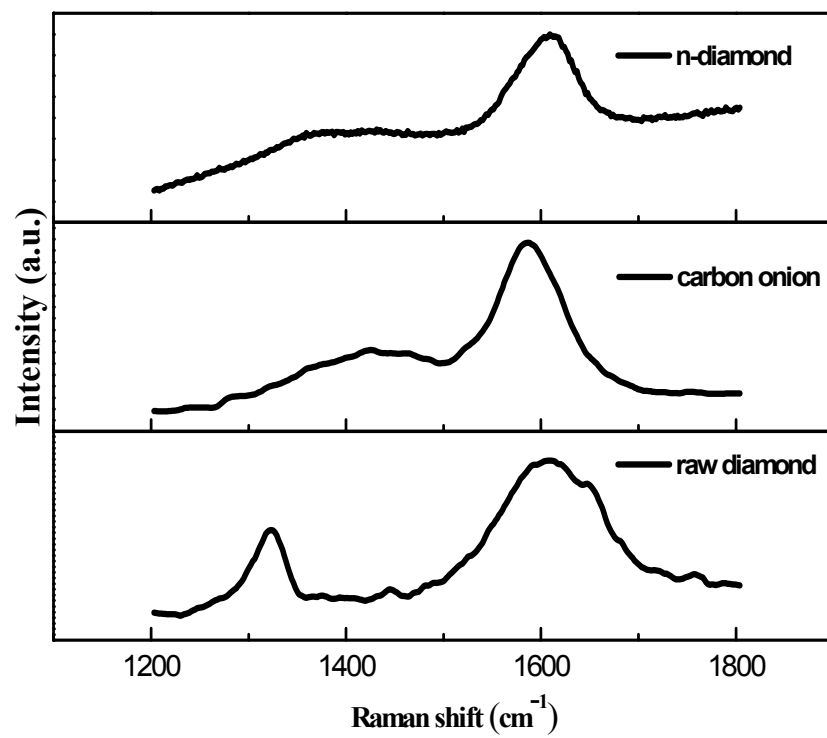


Figure 5

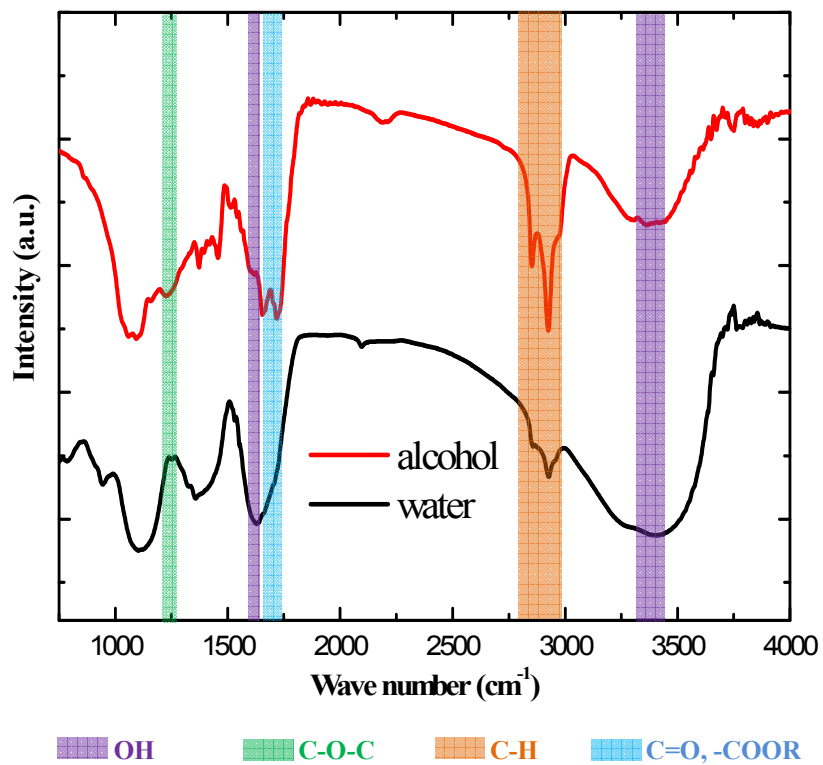


Figure 6

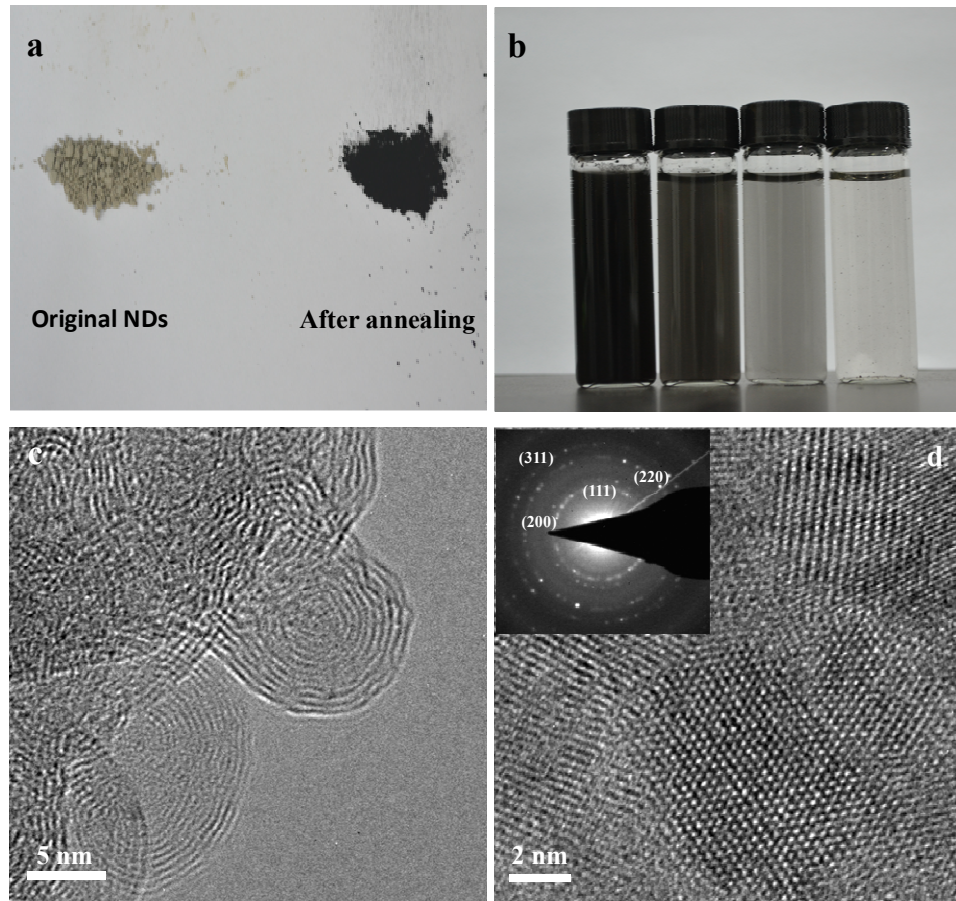


Figure 7

